A PHOTOELECTRON SPECTROSCOPIC INVESTIGATION OF VINYL FLUORIDE (C_2H_3F). THE HeI, THRESHOLD AND CIS PHOTOELECTRON SPECTROSCOPY.

R. Locht[1], B. Leyh,
Laboratoire de Dynamique Moléculaire, Département de Chimie,
Institut de Chimie, Bât.B6c, Université de Liège,
Sart-Tilman par B-4000 Liège 1, Belgium.
D. Dehareng
Centre d'Ingéniérie des Protéines, Institut de Chimie, Bât.B6a, University de Liège,
Sart-Tilman par B-4000 Liège 1, Belgium.
K. Hottmann and H. Baumgärtel
Institut für Physikalische und Theoretische Chemie,
Freie Universität Berlin, Takustraβe 3,
D-14195 Berlin, Germany.

ABSTRACT.

The threshold photoelectron spectrum (TPES) and the constant ion state (CIS) spectra of the individual ionic states of C_2H_3F have been recorded using synchrotron radiation. For comparison a well resolved HeI photoelectron spectrum (HeI-PES) has also been measured and analyzed in detail. The TPES has been measured between 9.5 eV and 35 eV photon energy. Numerous vibrational structures, reported for the first time, observed in the ground state and the six excited states of the cation are analyzed. Quantum chemical calculations have been performed and provide strong support to the assignments. State selected CIS spectra highlighted the major importance of autoionization for the production of almost all ionized states of C_2H_3F observed in this work.

1. INTRODUCTION.

The only photoelectron spectroscopic (PES) technique that has been applied to vinyl fluoride (C_2H_3F) is the fixed wavelength HeI-PES at 54.8 nm. The earliest well resolved HeI-PES of this molecular system has been reported by Lake and Thompson [1]. The vibrational structure observed in the first band has been analyzed and assignments have been proposed. The structureless photoelectron

[1] Corresponding author: R. Locht; e-mail: robert.locht@ulg.ac.be

bands observed at higher binding energies have been neither analyzed nor assigned.

Reinke et al. [2] shortly presented a well resolved HeI-PES for comparison purposes with their photoionization mass spectrometric work on C_2H_3F [3]. These authors performed a vibrational analysis of the first photoelectron band and proposed an interpretation of the higher energy bands observed in the spectrum.

The photoelectron spectroscopic work has been considerably extended in energy by the use of the HeII resonance line at 30.4 nm. This provided information on the binding energy of the inner-valence shell orbitals of the molecules. This technique was extensively applied by Bieri et al. [4,5], e.g. to fluoro-compounds. These authors presented the first HeII-PES of C_2H_3F and analyzed their experimental results based on quantum mechanical calculations.

Sze et al. [6] reported the investigation of the monohaloethylenes (C_2H_3X, X=F, Cl, Br, I) by using HeI and HeII PES and electron energy loss spectroscopy. These authors measured the ionization energies corresponding to the different photoelectron bands and analyzed the observed vibrational fine structure. The electron energy loss spectra were related to the vacuum UV photoabsorption spectra of the same molecular systems. The photoabsorption spectroscopic data related to C_2H_3Cl [7], C_2H_3Br [8] and C_2H_3F [9] have been analyzed in great detail and reported in earlier publications.

Several theoretical studies were devoted to the description of ethylene and its halogenated derivatives. Ab initio SCF-calculations have first been reported by Meza and Wahlgren [10] describing C_2H_4 and C_2H_3F. Ionization energies of the corresponding molecules were calculated.

Heaton and El-Talbi [11] reported ab initio molecular orbital calculations at the SCF level for the complete series of fluorinated ethylenes. Vertical ionization energies have been calculated and assignments of the experimental observations have been proposed.

Bieri et al. [4,5] and Potts et al. [12] extended their calculations to interpret the HeII-PES which also involves ionization from the inner-valence shell orbitals. Semi-empirical, HAM/3 and many-body Green's function calculations were used. Recently, Pradie and Linnert [13] performed new calculations of the first ionization

energies (adiabatic and vertical values) for fluorinated, chlorinated and chlorofluorinated ethylenes at the Hartree-Fock (HF) level using GTlarge and 6-311+G(3df,2p) basis sets. A critical review of the results was presented.

Takeshita [14] also proposed ab initio calculations on halogenated ethylenes. To the best of our knowledge, it is the only theoretical study investigating the molecular structures and the vibrational levels of the ground electronic state of the cation. This author compared the calculated results with the experimental intensities and wavenumbers.

We recently published a detailed investigation of the photoabsorption spectrum of C_2H_3F between 6 eV and 25 eV photon energy using synchrotron radiation [9]. To extend the study of this molecular system to its cationic states, their photoelectron spectra have been investigated and are described in the present paper. The fixed wavelength HeI-PES has been remeasured and has been completed by variable wavelength TPES (threshold photoelectron) and vibrationally resolved CIS (constant ion state) spectroscopy. These techniques are expected to highlight autoionizing contributions as well as dissociative ionization pathways of C_2H_3F.

2. EXPERIMENTAL.

2.1. Experimental setup.

The experimental setup used in this work has already been described in detail elsewhere [15]. Only the most important features of the three experimental techniques used in the present experiments will be reminded in this section.

Except for the HeI-PES measurements, in all experiments reported here we used the vacuum UV light from the synchrotron radiation provided by the electron storage ring BESSY (Berlin, Germany). This light is dispersed by a vacuum UV 3-meter normal incidence (3m-NIM beam line) monochromator [16] equipped with a 2 400 l/mm Pt-grating. The entrance and exit slit widths were set at 50 μm to 200 μm depending on the signal intensity.

The light beam is focussed into an ion chamber, in the focussing plane of a tandem electron spectrometer consisting of two 180° electrostatic deflectors. This electron energy analyzer works at constant pass energy E_0, leading to a constant

energy resolution. The resolution defined as the full width at half-maximum (FWHM) is given by $\Delta E/E_0=w/104$ where w is the slit width expressed in millimeters. In the present experiments w=0.5 mm or 1.0 mm and E_0 is set at values between 0.4 V and 10.0 V depending on the type of experiment and on the signal intensity.

In addition to the synchrotron storage ring beamcurrent, the photoelectron signal of a gold diode, inserted in the ion chamber at the opposite of the 3m-NIM monochromator exit slit, is measured in order to normalize the photoelectron signals in the TPES and CIS spectra.

The first and most obvious operating mode of this experimental setup is the measurement of "fixed-wavelength" photoelectron spectra. The HeI resonance line at 58.4 nm is produced in a microwave discharge and guided into the ionization region through a quartz capillary. Optimal conditions for resolution and intensity are obtained for a pass energy E_0=0.4 V providing a nominal resolution of 16 meV as measured on the $Xe^+(^2P_{3/2})$ peak.

The second operating mode is the measurement of "constant photoelectron energy" spectra. These are recorded by tuning the photon energy $h\nu$ and keeping constant the energy E^e_{kin} of the electrons transmitted through the tandem electron energy analyzers system. To transmit only "zero-kinetic energy" or "threshold" (TPE) photoelectrons, the electron accelerating voltage V_{acc} is kept equal to E_0 as close as possible. This equality is optimized to obtain the highest TPE signal intensity. The TPE of the sample gas has been normalized to the photon transmission function of the monochromator by measuring simultaneously the photoelectron current intensity of the gold diode.

The third kind of experiment performed with this instrument is the "constant ion state" (CIS) spectroscopy of vibrational and/or electronic states of molecular ions. The aim of this experiment is to measure the relative partial ionization cross-sections as a function of the photon energy for well-defined vibronic states of the molecular ion. Autoionization is well known to strongly perturb photoionization and dissociative photoionization cross-sections by inducing dramatic variations in the distributions of the final ionic states. Recording a CIS spectrum requires to keep $IE=h\nu-E^e_{kin}$ constant, i.e., the ionization energy corresponding to the considered ionic state. The photon energy $h\nu$ and the photoelectron kinetic energy E^e_{kin} must therefore be scanned in parallel. The details about the experimental procedure have

been described earlier [15].

The commercially available C_2H_3F, purchased from Fluochem Ltd and of 99.5% purity, was used without further purification.

2.2. Data handling and error estimation.

To improve the experimental resolution of the HeI-PES, the original spectrum has been deconvoluted. A repeated iterative procedure [17] has been used, improving the effective resolution down to about 8 meV, as mesured on the PES of C_2H_3F.

As will be discussed in the next sections, weak structures and diffuse peaks are often superimposed on a strong continuum. To make the characterization of these features easier a "continuum subtraction" procedure has been applied. This method has already been used successfully in previous spectral analyses [18]. For this purpose, the experimental curve is severely smoothed to simulate the underlying continuum which is then subtracted from the original photoabsorption spectrum. The smoothing procedure consists in filtering the experimental curve by fast Fourier transform (FFT). The weak features emerge from a strongly attenuated remaining background. The resulting diagram will be called Δ-plot in the forthcoming sections.

In the HeI-PES, the photoelectron energy scale has been calibrated by recording the PES of a rare gases X-C_2H_3F mixture (X=Ar, Kr and Xe). The rare gas ionization energies corresponding to the $^2P_{3/2}$ and $^2P_{1/2}$ ionic states are used to carry out a linear regression giving ±2 meV precision of the energy scale. Under high resolution conditions, the spectrum has been scanned with 1 meV increments.

The photon energy scale of the 3m-NIM monochromator has been calibrated with rare gas photoabsorption and/or threshold photoelectron spectra. An accuracy of better than 2-3 meV is achieved. For this purpose Ar and/or Xe were used. To obtain the relative partial photoionization cross-sections, the CIS spectra have to be normalized to the transmission functions of the monochromator and of the electron energy analyzer. The former is recorded simultaneously with the CIS spectrum. The latter is obtained by recording the CIS curve of a rare gas, e.g. Xe^+ ($^2P_{3/2}$) exhibiting no structure over the same photon energy range as for the investigated molecular ion.

The error on the energy position of a feature is estimated to be 6 meV when the spectrum is recorded with energy increments of 4 meV, i.e., in the TPES and HeI-PES over large energy ranges. For the broad bands observed in these spectra, the positions of the maxima (vertical ionization energies) are estimated with an accuracy of 10 meV. In the photoelectron spectra recorded with 1 meV increments over narrow energy ranges, the accuracy is estimated to be of about 4 meV including the energy scale precision. For the CIS spectra recorded with 10 meV increments, the positions of the features are measured with an error estimated to be 15 meV.

3. EXPERIMENTAL RESULTS.

For the easiness of the discussion the HeI, TPES and CIS spectra will be discussed separately.

3.1. The HeI and Threshold photoelectron spectra.

The TPE spectrum of C_2H_3F has been recorded over a wide photon energy range, i.e., 8 eV to 35 eV. The upper limit was defined by the grating transmission function.

FIG. 1.

The photon monochromator and the electron spectrometer have been tuned for medium resolution conditions, i.e., 200-200μm slit widths and 5 eV pass energy respectively leading to an overall resolution of about 25 meV. The restricting effect on the overall resolution of the present photon monochromator settings is clearly illustrated in Fig. 1: the first PE band is recorded using the same electron spectrometer conditions for both the PES and the TPES spectra. Fig. 2a shows the TPE spectrum extending up to 30 eV photon energy and recorded with 4 meV energy increments.

FIG. 2.

Nine well-defined bands are observed at vertical ionization energies of 10.570±0.006 eV, 13.76±0.01 eV, 14.56±0.01 eV, 16.64±0.01 eV, 17.84±0.01 eV,

20.18±0.01 eV and at about 22.7 eV, 24.5 eV and 26.7 eV. Emerging slightly from the noise level, a very weak band could be observed near 30.1 eV. A fairly strong feature is noteworthy to mention at about 12.6 eV as a shoulder of the very strong band at 13.76 eV.

For comparison the HeI-PES of C_2H_3F has been recorded over the whole ionization energy region available with the HeI resonance line and at medium resolution, i.e., with a pass energy E_0= 2.1 eV. The typical result is shown in Fig. 2b where the energy increment is 7 meV. In this spectrum the vertical ionization energies are measured at 10.554±0.006 eV, 13.79±0.01 eV, 14.53±0.01 eV, 16.71±0.01 eV, 17.91±0.01 eV and at 20.20±0.01 eV. Shoulders are observed at about 16.16 eV and 19.67 eV.

TABLE 1.

In Table 1, the HeI- and HeII-PES results reported in earlier papers [1,2,4-6] are compared with the HeI and with the TPES results of the present work.

Two remarkable differences have to be noticed between the HeI-PES and the TPES. Several features, such as the shoulders at about 16.16 eV and less clearly at about 19.67 eV, are present in the HeI-PES but neither is observed in the TPES spectrum. A relatively strong shoulder at 12.6 eV is clearly observed in the TPES and not observed in the HeI-PES. The second important difference between the two spectra is the dramatic differences of ionization cross-sections of the different ionic states. The HeI-PES is dominated by the ground state whereas in the TPES the first four excited states dominate the spectrum.

3.2. The CIS photoelectron spectra.

The CIS spectra were recorded over an energy range of 10 eV, i.e., from the $\tilde{X}\,^2A''$ threshold up to 24 eV photon energy. Owing to the weakness of the signal, these time-consuming measurements were restricted to the strongest features in the TPES. For the ionic $\tilde{X}\,^2A''$ ground state the CIS spectra were measured for the first four ν_4 vibrational levels. No noteworthy differences between these curves have been observed and Fig.3a shows a typical CIS spectrum for the v=1 level of ν_4 in the $C_2H_3F^+(\tilde{X}\,^2A'')$ ground ionic state.

FIG. 3.

The same figure shows the CIS measurements for the successive electronic ionic states observed in the TPES up to 20 eV. Remarkably, the shape of the spectra corresponding to the 13.76-14.56 eV and to the 16.6-17.84 eV pairs of states, are very similar. In all these curves only broad structures are observed. For the easiness in the interpretation and discussion, the photoabsorption spectrum of C_2H_3F measured in the same energy range [9] has been added to the figure (Fig. 3b).

4. AB INITIO CALCULATIONS. Methods and Results.

4.1. Computational tools.

The basis set used is cc-pVTZ [19,20], i.e., a valence triple ζ-basis set with polarization functions. The geometry optimizations of the neutral and the two lowest electronic states of the cation as well as the wavenumbers calculations of their corresponding vibrational normal modes were performed at the B3LYP level [21,22]. Some excited state geometries were optimized at the CIS (Configuration Interaction with Single excitation) level [23] and at the CASSCF (Complete Active Space Self Consistent Field) level [24-26]. Most of the CASSCF calculations involve eight active orbitals and eleven electrons [CAS(11,8)]. Some calculations were also performed in CASSCF with seven active orbitals and seven electrons [CASSCF(7,7)].

For the CASSCF calculations, the geometry optimizations were performed with or without state average option which means that the molecular orbitals were optimized by taking into account (or not) all the states involved in the calculation. The wavenumbers calculations were performed without this option. An avoided crossing between the $\tilde{A}\,^2A'$ and the $\tilde{B}\,^2A'$ states and a conical intersection between the $\tilde{B}\,^2A'$ and the $\tilde{C}\,^2A''$ states were searched out.

All calculations were carried out with the GAUSSIAN 03 programme [27].

4.2. Results of the Calculations.

The parameters of the optimized geometry as calculated for the ground state and the first two ionic states at the B3LYP//cc-pVTZ level are listed in Table 2.

TABLE 2.

The calculated vertical (adiabatic) ionization energies obtained for the ground ionic state $\tilde{X}\,^2A''$ and the first excited ionic state $\tilde{A}\,^2A'$ are equal to 10.49 (10.17) eV and 13.51 (12.91) eV respectively.

The optimized geometries at the CAS(12,8) or CAS(11,8) level for the neutral molecule and the molecular ion respectively, with or without the state average option, are summarized in Table 3.

TABLE 3.

The results of the B3LYP calculations of the wavenumbers characterizing the twelve vibrational normal modes represented in Fig. 4 are listed in Table 4 for the $\tilde{X}\,^1A'$ neutral

FIG. 4.

TABLE 4.

ground state and the $\tilde{X}\,^2A''$ ionic ground state. For the ionic excited states of C_2H_3F, the wavenumbers were calculated at the CAS(11,8) level and the results are listed in Table 5. A comparison between the results obtained at both the B3LYP and CAS(11,8) levels for the $\tilde{A}\,^2A'$ ionic state is shown in the same Table.

TABLE 5.

The geometry optimization of the $\tilde{D}\,^2A'$ state was rather difficult because of the many intersections encountered on the way to its optimal configuration. This state is a dissociative state leading to $C_2H_3^+$ ($^1A'$) and F (^2P) and is degenerate with the $\tilde{A}\,^2A'$ state at the dissociation asymptote. During the CIS optimization of the $\tilde{B}\,^2A'$ state, a crossing with the $\tilde{A}\,^2A'$ state occurred and this second excited state becomes therefore the first excited state. Therefore, the geometry of the lowest energy point for the avoided crossing between the two states has been searched out. Similarly, the optimization of the $\tilde{C}\,^2A''$ pointed out to the existence of a conical intersection between the $\tilde{B}\,^2A'$ and the $\tilde{C}\,^2A''$ states: the geometry at this intersection has also been optimized. The optimization of the $\tilde{D}\,^2A'$ state also revealed several intersections but it was not possible to obtain a converged geometry, i.e., a geometry for which the energy gradient was numerically equal to zero. However, on the optimization pathway, some geometries corresponding to very small energy

differences (0.0001 a.u.) were found though they were characterized by a large gradient and thus did not correspond to the lowest energy points. The calculated parameters are listed in Table 6.

TABLE 6.

5. DISCUSSION OF THE EXPERIMENTAL DATA.

5.1. The HeI photoelectron spectrum.

In terms of molecular orbitals, restricted to the outer-valence and inner-valence shell orbitals, the electronic structure of C_2H_3F in its ground electronic state $\tilde{X}\,{}^1A'$ in the C_S symmetry group is represented by [9]

$$(1a')^2\,(2a')^2\,(3a')^2\,(4a')^2\,(5a')^2\,(1a'')^2\,(6a')^2\,(7a')^2\,(2a'')^2 : \tilde{X}\,{}^1A'$$

The inner-shell atomic-like orbitals are the $F(1s)^2$, $C_1(1s)^2$ and $C_2(1s)^2$. The occupied a″ orbitals have a π character: the 2a″ is a C=C bonding orbital whereas the 1a″ is a C-F bonding orbital. All the na′ orbitals have a σ character.

The medium resolution HeI-PES shown in Fig. 2b is in good agreement with previous observations [1,2,6]. As already mentioned, this spectrum is dominated by the first band observed at 10.56 eV and made of sharp and strong structures. At medium resolution the second, and the fourth to sixth bands look structureless. Presumably, in the last band at about 20.2 eV, a weak structure is visible. All these features are characterized by their vertical ionization energy listed in Table 1. Fairly good agreement is found with previously reported data [1,2,4-6]. However, two additional structures or unresolved bands are clearly observed as shoulders at about 16.2 eV and 19.7 eV successively. These structures have never been mentioned in earlier publications.

The HeI-PES has also been measured under higher resolution conditions by reducing the pass-energy E_0 of the electron energy analyzer to E_0=0.39 eV. The result on the first PES band is shown in Fig. 5 which can be directly compared with the result

FIG. 5.

shown in Fig. 1: the resolution increase is obvious. To improve the experimental resolution the deconvolution method has been applied (see section 2.2). The result is also shown in Fig. 5 and an effective resolution of 8 meV is obtained. The energy positions of the structures observed in the first band have been listed in Table 7.

TABLE 7.

This band is assigned to the ionization of the highest occupied 2a″ orbital with a predominant C=C π orbital character giving rise to the $\tilde{X}\,^2A''$ ground state of the $C_2H_3F^+$ cation. The experimental adiabatic and vertical ionization energies (IE) are $IE_{ad}(C_2H_3F^+, \tilde{X}\,^2A'')$=(10.363±0.004) eV and $IE_{vert}(C_2H_3F^+, \tilde{X}\,^2A'')$=(10.558±0.004) eV respectively. The literature data on the adiabatic IE as measured directly by photoelectron spectroscopy are very scarce. The value of 10.37 eV is reported by Lake and Thompson [1] and Reinke et al. [2] without any uncertainty indication. Theoretical calculations predicted this quantity to be at 10.27 eV [10], 10.37 eV [13] and 8.83-9.60 eV [14] depending upon the calculation level. The experimental vertical ionization energy values are in good agreement, except for the values determined by HeII-PES [4,5] showing a systematic higher value compared to that obtained by HeI-PES.

The vibrational structure observed in the $\tilde{X}\,^2A''$-band of $C_2H_3F^+$ has been assigned to progressions essentially involving four vibrational normal modes: ω_4= 1565±16 cm^{-1} (194±2 meV), ω_7= 1274±12 cm^{-1} (158±1.5 meV), ω_9= 500±32 cm^{-1} (62±4 meV) and two alternatives for the value of ω_8, i.e., 839±40 cm^{-1} (104±5 meV) or 968±30 cm^{-1} (120±4 meV). In this band overtones and combinations are observed. Table 7 displays the assignments proposed for almost all structures observed in the first PES band. Several assignments are indicated in italic corresponding to (i) an alternative and very reproducible value of ω=104±5 meV (with overtones and combinations of it) and (ii) more complex combinations, i.e., of three normal modes. In both cases, the corresponding expected energy position is calculated by using the theoretical values of the wavenumbers obtained in this work and is indicated in brackets. These experimental results and the theoretical values of the wavenumbers are summarized in Table 8 including the available

TABLE 8.

literature data. For the wavenumber associated with ν_4 two distinct values are

measured, i.e., 1 530 cm^{-1} [1,6] and 1 570 cm^{-1} [2] or 1 565±16 cm^{-1} (present work). Considering the accuracy on the present value, good agreement is found with the experimental determination in ref. [2] only and with our calculated theoretical value of 1 567 cm^{-1}. The same consideration is valid for the wavenumber characterizing ν_7 for which 1 330 cm^{-1} [1,2] and 1 270 cm^{-1} [6] or 1 274±12 cm^{-1} (present work) were determined. In this case, very good agreement is noted with the measurement of ref. [6] only, and with the present theoretical prediction at 1 246 cm^{-1}. The discrepancy of about 50 cm^{-1} with the determinations of Lake and Thompson [1] and Reinke et al. [2] is fairly large and outside the uncertainty limits. The different works agree for ν_9 for which ω_9= 500 cm^{-1} is measured.

However, if the latter assignment, i.e., ω_9= 500±32 cm^{-1}, is unambiguous, its second and higher overtones and combinations are not (see in italic in Table 8). The reason is that the predicted values (see Table 4) for 2.ω_9= 2x489 cm^{-1} and ω_8= 984 cm^{-1} are very close: these two values are indistinguishable in the present experiment.

The second questionable assignment is ω= 839±40 cm^{-1} which is observed with overtones and combinations. This wavenumber has also been detected unambiguously in the Rydberg series converging to the $C_2H_3F^+$ ($\tilde{X}\ ^2A''$) cationic state [9]. In their HeI-PES Sze et al. [6] mentioned also a wavenumber of 850 cm^{-1} and assigned it to CH_2 deformation (see Table 1 in ref. [6]). The assignment to ν_8 would imply a fairly large discrepancy with the predicted value of 984 cm^{-1} (see Table 4) and the observed low wavenumber would require a C-F bond weakening. This is in contradiction with the predicted C-F bond shortening resulting from the 2a″ ionization. The best alternative assignment based on the present calculations would be the ν_{11}(a″) vibrational motion (involving H out-of-plane deformations) for which ω_{11}= 873 cm^{-1} has been calculated (see Table 4). Such a forbidden transition would only be allowed by a vibronic coupling. The weakness of the transition could support this interpretation.

The deconvoluted HeI-PES of C_2H_3F above 13 eV is displayed in Fig. 6a where clearly six vibronic bands are observed. The most intense band maxima are measured at 13.79±0.01 eV, 14.53±0.01 eV, 16.71±0.01 eV, 17.91±0.01 eV and 20.20±0.01 eV

FIG. 6.

successively. A shoulder located at 16.1 eV is observed in the 16.71 band. Likely a

weak band is partially hidden at around 19.7 eV in the 20.2 band. In spite of the resolution obtained in the present measuring conditions (about 12 meV) most of these bands exhibit only very partially resolved structures. The resolution is likely to be limited by the natural linewidth of the vibrational states which is related to their lifetime.

In a recent analysis of the vacuum UV photoabsorption spectrum of C_2H_3F [9], several structured broad bands were observed near and above 11 eV, i.e., at 10.94 eV, 11.3 eV, 12.5 eV and 12.9 eV. These were possibly assigned to 3s, 3p and 3d Rydberg series converging to the 13.79 eV ionization limit. Diffuse features were mentioned but neither classified nor assigned. The present data could provide more detail on these structures.

Applying the continuum subtraction method to the PES, the resulting Δ-plot is shown in Fig. 6b revealing more clearly the fine structure present in these bands. The energy positions of these features are listed in Table 9.

TABLE 9.

For the PE-band with its maximum at 13.79 eV, an adiabatic ionization energy (IE_{ad}) could be measured at IE_{ad}= 12.953±0.010 eV. From most of the literature data [1,2,4,6] (see Table 1), only the vertical ionization energy (IE_{vert}) is available as lying at IE_{vert}= 13.8 eV, in very good agreement with the present measurements. Only Reinke et al. [2] obtained an IE_{ad}= 13.27 eV by using an extrapolation method. By quantum mechanical calculations [4,5], IE_{vert}= 13.8 eV is obtained and assigned to the $(7a')^{-1}$ ionization leading to the $\tilde{A}\,^2A'$ first excited ionic state. In the present work, the calculations provide IE_{ad}= 12.91 eV and IE_{vert}= 13.51 eV.

The Δ-plot related to this band is shown in Fig. 7a on an expanded ionization energy scale. A classification of most of the features observed between 12.9 eV and 14.3 eV has been attempted and has been assigned to a vibrational progression. Very likely the 13.8 eV-band is made of two parts: (i) the low-energy 12.9-13.6 eV part showing a regular structure made of progressions with two average wavenumbers ω_A= 110±10 meV (887±80 cm^{-1}) and ω_B= 54±6 meV (435±48 cm^{-1}) and (ii) the 13.9-14.2 eV part showing a short progression with ω= 140±10 meV (1 129±80 cm^{-1}). The broad and strong structures do not fit in these regularities.

FIG. 7.

As mentioned above, the wavenumber ω_A= 110±10 meV is an average value. It is possibly affected by a strong anharmonicity. Using the data listed in Table 9 (for the first five ν_A values, a Birge-Sponer plot (with 0.92 correlation coefficient) provides ω_A= 129±4 meV (1 040±32 cm^{-1}) and $\omega_A x_A$= 3.1±0.6 meV (25±5 cm^{-1}). Comparing the wavenumber values below and above the 13.6-13.9 eV region, it could be suggested that one is dealing with the same vibrational normal mode.

For the assignment of ω_A and ω_B we can only refer to the quantum mechanical calculations performed in the present work. Wavenumbers related to the $\tilde{A}\,^2A'$ state of $C_2H_3F^+$ have been calculated at different levels and the results are listed in Table 4. Unambiguously the ω_B= 435±48 cm^{-1} determined by PES fits at best the predicted 428 cm^{-1} value for ω_9 ascribed to the CH_2 in-plane rocking and F-CC bending motion.

Concerning the wavenumber ω_A= 1 040±32 cm^{-1}, it has to be compared with the predicted ω_4= 1 074 cm^{-1} and ω_5= 1 176 cm^{-1} involving H-CC bending and C-F stretching respectively. Within the uncertainty limits on the experimental determination, ω_4 would best correspond to ω_A but ω_5 could not be discarded, because the accuracy of the quantum chemistry calculations is not known. Referring to Table 2, the $\tilde{X}\,^1A' \rightarrow \tilde{A}\,^2A'$ transition involves strong changes in the C-F bond length and in the H-CC angles so that both normal modes could show extended progressions.

The 13.6-13.9 eV region (in italic in Table 9) shows at least four features difficult to integrate in the above mentioned progressions. As a matter of fact, an assignment in terms of vibrational normal modes is probably irrelevant here, because this region of the $\tilde{A}\,^2A'$ hypersurface is strongly perturbed by nonadiabatic interactions. From photoion-photoelectron coincidence (PIPECO) measurements [28] and dissociative photoionization mass spectrometric data [29] the four most important fragmentation channels of $C_2H_3F^+$ are open and in competition. The appearance energies for $C_2H_2^+$, $C_2H_2F^+$, C_2HF^+ and $C_2H_3^+$ are respectively 13.51 eV, 13.64 eV, 13.72 eV and 13.84 eV [29]. They represent 60% of the total ionization measured at 20.7 eV [29]. A more accurate description of the strongly perturbed 13.6-13.9 eV region must very likely take into account the avoided crossing between the $\tilde{A}\,^2A'$ and the $\tilde{B}\,^2A'$ states of $C_2H_3F^+$ ion identified by the present calculations (see section 4.2).

The PE band extending from 14.3 eV to 15.5 eV exhibits a more regular structure (see Fig. 6) giving rise to a fairly well structured Δ-plot shown in Fig 7a. The energy positions of the features are listed in Table 9. The adiabatic ionization energy could not be measured. Therefore, we started the analysis at 14.342 eV which corresponds to an excited vibrational level, whose energy is noted E_{min}, of the considered excited state of the $C_2H_3F^+$ ion.

This band is assigned to the $(6a')^{-1}$ ionization and corresponds to the $\tilde{B}\,^2A'$ state of $C_2H_3F^+$ in agreement with previous calculations [4,10]. A fairly simple progression likely involving a single vibrational normal mode is observed. The average spacing is ω= 110±17 meV (887±130 cm^{-1}). This experimental value falls between two ab initio calculated values (see table 5), i.e., ω_7= 1 094 cm^{-1} and ω_8= 529 cm^{-1} using CAS(11,8) level calculations. Comparing the results for the wavenumbers characterizing the $\tilde{A}\,^2A'$ state of $C_2H_3F^+$ (see Table 5) calculated at different levels, the CAS(11,8) level calculations provide ω values exceeding the B3LYP values by about 5-18%. This finding would argue for assigning ω= 887±130 cm^{-1} to the ν_7 mode corresponding to the H-CC bending excitation.

It is noteworthy to mention that the $\tilde{B}\,^2A'$ PES band exhibits a fairly regular intensity distribution except for $E_{min}+3\nu_7$ at 14.672 eV. This member corresponds almost exactly to the energy range where two appearance energies, that is $AE(CH_2F^+)$= 14.60 eV and $AE(CF^+)$= 14.74 eV, have been measured [29]. Furthermore, the perturbation of the $\tilde{B}\,^2A'$ state by an avoided crossing with the $\tilde{A}\,^2A'$ state and by a conical intersection with the $\tilde{C}\,^2A''$ state has been established by the present ab initio calculations (see section 4.2). Dissociative autoionization could also be invoked (see region c in the PAS, Fig. 3b).

As already pointed out, Fig. 6a very clearly shows the existence of a strong shoulder PES-band at about 16.16 eV. Sze et al. [6] also mention a PES band at 16.0 eV.

According to the present ab initio quantum mechanical calculations, the 1a″ orbital comes immediately below the 6a′ orbital. Ionization from this orbital leads to the $\tilde{C}\,^2A''$ ionized state of $C_2H_3F^+$. In their photoelectron spectroscopic and theoretical work, Bieri et al [4] assigned the 16.7 eV band to the $\tilde{C},\tilde{D}$ (1a″,5a′) ionizations measured at 16.7 eV and calculated at 16.79 eV and at 17.13 eV respectively. Heaton and El-Talbi [11] calculated the $(1a'')^{-1}$ and the $(5a')^{-1}$ ionization

energies at about 17.0 eV. Sze et al. [6] reversed the 5a′ and 1a″ orbitals ionization energies, i.e., $(5a')^{-1}$ and $(1a'')^{-1}$ were assigned to 16.0 eV and 16.7 eV respectively.

An attempt to analyze the structure of the $\tilde{C}\,^2A''$ band is presented in Table 9 extending from 15.511 eV up to 16.120 eV. As shown in Fig. 7b probably three different vibrational normal modes are involved and are characterized by ω_A= 230±10 meV (1 855±80 cm^{-1}), ω_B= 147±25 meV (1 185±200 cm^{-1}) and ω_C= 76±8 meV (613±64 cm^{-1}). The predicted wavenumbers as calculated at the CAS(11,8) level are listed in Table 5. Taking into account the above mentioned remark about the CAS and B3LYP calculation levels, the ω_A and ω_C could very likely be assigned to the ν_4 (C=C stretching) and ν_8 (C-F stretching and CH_2 rock in-plane) vibrational motions, respectively calculated at ω_4= 1 793 cm^{-1} and ω_8= 500 cm^{-1}. The assignment for the less accurate ω_B=1 185 cm^{-1} could be ω_6= 1 276 cm^{-1}.

The adiabatic ionization energy of the next PES-band having its vertical ionization energy at 16.71 eV is estimated to be IE_{ad}= 16.0 eV by linear extrapolation of the peak low-energy side. Reinke et al. [2] reported IE_{ad}= 16.14 eV. It should be assigned to the $(5a')^{-1}$ orbital ionization resulting in the $\tilde{D}\,^2A'$ state formation of $C_2H_3F^+$.

An attempt to disentangle the vibrational structure from the Δ-plot shown in Fig. 7b is presented in Table 9. Very likely three wavenumbers would account for most of the features, i.e., ω_A= 220±7 meV (1 774±56 cm^{-1}), ω_B= 142±17 meV (1 145±150 cm^{-1}) and ω_C= 80±12 meV (645±100 cm^{-1}). The largest wavenumber seems to be characterized by a fairly strong anharmonicity and the Birge-Sponer diagram (with 0.90 correlation coefficient) provides $\omega_A x_A$= 4.5± 1.2 meV (36±10 cm^{-1}). This observation could be linked to a strong perturbation of the $\tilde{D}\,^2A'$ hypersurface by, e.g., a conical intersection and/or an avoided crossing as mentioned at the end of section 4.2. A similar phenomenon was already pointed out for the $\tilde{A}\,^2A'$ state of $C_2H_3F^+$.

The difficulties encountered in the calculation of the $\tilde{D}\,^2A'$ state, owing to the multiple surface crossings prevented us from calculating the vibrational wavenumbers (see section 4.2). This state was found to be a transition state (see TS in table 5: presence of an imaginary wavenumber) in the C_S symmetry group. Experimentally, the ω_A= 1 774±56 cm^{-1} could very probably be assigned to the C=C or C-H stretching motion, whereas ω_C= 645±100 cm^{-1} would likely involve an H-CC bending motion and ω_B= 1 260 cm^{-1} could be related to the C-F stretching vibration.

The PE band with its IE_{vert}= 17.91±0.01 eV is assigned to the $(4a')^{-1}$ ionization predicted at 18.34 eV by theoretical calculations [4] and giving rise to the $\tilde{E}\,^2A'$ state of the $C_2H_3F^+$ ion.

In a first part, spreading up to 17.998 eV, this band seems to consist of one progression with ω_A= 98±8 meV (790±64 cm^{-1}) and its combination with ω_B= 47±10 meV (379±80 cm^{-1}). If the latter wavenumber can very likely be assigned to ν_9 (CH_2 in-plane rocking), the former lies in the range of the ν_7 (H-CC bending) frequency, as observed for most of the lower lying ionic states.

Surprisingly, the ω_A= 98±8 meV progression is interrupted at 18.068 eV where a sudden intensity increase is observed highlighting a short progression with a larger wavenumber ω_C= 123±6 meV (992±48 cm^{-1}) which likely involves the C-F stretching motion.

Quantum mechanical calculations predicted the $(3a')^{-1}$ orbital ionization energy at 20.86 eV [4]. The PES band observed at 20.2 eV was then assigned to the corresponding $\tilde{F}\,^2A'$ state [4]. This energy corresponds to the band observed at 20.20±0.01 eV in the present work but denoted $\tilde{G}\,^2A'$ in Fig. 6. This band shows two characteristics never mentioned earlier: it exhibits (i) a well defined vibrational structure (see Fig. 6b) and (ii) a weak shoulder extending between 19.1 eV and 19.8 eV (see Fig. 2b and Fig. 6a).

Table 9 and Fig. 6b clearly show the regular vibrational progression involving a single wavenumber ω_A= 120±8 meV (968±32 cm^{-1}) and starting at 19.917 eV. It can reasonably be assigned to a ν_7 vibration involving the H-CC bending motion.

The Δ-plot in the weak shoulder region (see Fig. 6b) is fairly noisy compared to the range below 13 eV: no regular structure could be observed. However, undoubtedly a $C_2H_3F^+$ excited vibronic state is concerned. The relative weakness of the transition could indicate that a first multiple electron transition is involved: we refer to it as $\tilde{F}$ state in Fig. 6a. Alternatively, it could be assigned to the $(3a')^{-1}$ ionization leading to the $\tilde{F}\,^2A'$ state. Consequently, the upper structured band would then be assigned to the $(2a')^{-1}$ ionization giving rise to the $\tilde{G}\,^2A'$ state which is predicted to be at 24.76 eV [4].

5.2. The TPE and CIS Photoelectron spectra.

The TPES of C_2H_3F, recorded between 8 eV and 32 eV, is shown in Fig. 2a. Except for the relative intensities of the bands the TPE spectrum reproduces almost the HeI PE spectrum. However, in the 12 eV photon energy range, a quite strong band appears in the TPES only. Additionally, data are obtained above the 21.22 eV energy limit.

Dramatic intensity variations are observed between both spectra. When normalizing the intensity to the $\tilde{X}\,^2A''$ band, the $\tilde{A}$ to $\tilde{G}$ bands show large intensity increases of at least a factor 3 ($\tilde{E}$ state) to 9 ($\tilde{B}$ state). Clearly the intensity ratios within the two spectra are strongly perturbed also, e.g., $\tilde{A}/\tilde{B}$ intensity ratio being 1.6 in the HeI-PES and 0.8 in the TPE spectrum.

Except for the first $\tilde{X}\,^2A''$ band, the bands lying at higher energy are structureless at the resolution achieved in the present experiment. The result for the first band is shown in Fig. 1 and the position in energy of the features resolved in the TPES, are listed in Table 7. Good agreement is found between both HeI-PES and TPES experiments for the features observed under the present experimental conditions. Their assignments have already been discussed in detail (see section 5.1). Concerning the relative intensities of the individual vibronic transitions no significant differences have to be mentioned.

Contrary to the well of the $\tilde{X}\,^2A''$ potential hypersurface, its upper part can only be populated by autoionization. A fairly strong intensity increase of the threshold electron signal starts at 11.7 eV and a maximum is observed at 12.6 eV. Obviously this phenomenon is correlated with the presence of Rydberg states observed in the b-region of the photoabsorption spectrum (PAS) shown in Fig. 3b [9]. Owing to the large density of states, the fine structure could not be resolved.

At higher photon energies between 14 eV and 22 eV band maxima corresponding to vertical ionization energies have been measured (see Table 1) and good agreement is found with the HeI-PES results. Above 20.2 eV very weak transitions are observed corresponding to broad structureless bands in the TPE spectrum. The energy positions are listed in Table 1.

Ionization from the $(1a')^{-1}$ inner-valence shell orbital has been calculated to appear at 39.56 eV [4], i.e., too high for the observed structures. The weakness of

these transitions suggests that forbidden multiple electron transitions are involved. Sze et al. [6] investigated the HeII-PES of C_2H_3F but reported only the analysis up to 22 eV.

The large relative intensity variations (and ionization cross sections) between the HeI- and TPE spectra could only be interpreted with the help of both the CIS and the PAS spectra [9]. Both are shown in Fig. 3a and 3b in the 10-24 eV photon energy range. Five spectral regions (designated a-e) are related to energy ranges where Rydberg and/or valence transitions have been observed. The details of their assignment were discussed in an earlier work [9].

Vibrationally resolved CIS spectra have been recorded for the $\tilde{X}\,^2A''$ vibronic states and a typical example is shown in Fig. 3a. The $C_2H_3F^+$ vibronic state at 10.55 eV shows a fairly constant cross section over the wide 10.55-15.8 eV photon energy range. Only very weak b- and c-region contributions could be mentioned. Above 15.8 eV a strong cross section increase is observed corresponding to the d-region of the PAS which is linked to the ($\tilde{D}\,^2A'$)4s or 4d Rydberg state. This state autoionizes to the $\tilde{X}\,^2A''$ (ν_4, v=1) state of the cation. As will be reported later [30], this situation will drastically change with further fluorine-substituted ethylenes.

At higher photon energies the CIS spectra were recorded at the successive vertical ionization energies corresponding to the $\tilde{A}$ to $\tilde{G}$ cationic states (see Fig. 3a). The present data particularly highlight the contributions of the neutral excited states to the cross sections variations for the production (and dissociation) of each individual ionic state.

The nature of the neutral states involved in the transitions observed in the 10-22 eV photon energy has been discussed in detail (see Table 1 in ref. [9]). Several excited valence and Rydberg transitions have been identified and were assigned to the successive features observed in the PAS. Most likely the Rydberg states thus observed contribute significantly to the ionization cross section of C_2H_3F in its successive ionic states through autoionization. This latter phenomenon has to play an essential role, representing about 70%-90% of the total ionizing contribution as is the case for the $\tilde{A}-\tilde{E}$ ionic states.

6. CONCLUSIONS.

The HeI photoelectron (HeI-PES), threshold photoelectron (TPES) and constant ion state (CIS) spectroscopies have been applied for the detailed investigation of the photoionization of C_2H_3F. These techniques completed a previous investigation of the vacuum UV photoabsorption spectrum (PAS) of the same molecule [9]. The use of a subtraction method applied to the spectra allowed us to make a detailed examination of the abundant vibrational structure observed in the different PE bands. Ab initio quantum mechanical calculations applied to the $C_2H_3F^+$ system proved to be essential for the assignment of the numerous structures present in the spectra. Several perturbations in the vibrational structure observed in various PE bands could be linked to the opening of fragmentation channels as well as to the presence of conical intersections and/or avoided crossings identified by the quantum mechanical calculations.

ACKNOWLEDGMENTS.

We are indebted to the University of Liège, the Fonds de la Recherche Fondamentale Collective (FRFC) and the Freie Universität Berlin for financial support. R.L., B.L. gratefully acknowledge the European Community for its support through its TMR (Contract EU-HPRI-1999CT-00028) and I3 (Contract R II 3 CT-2004-506008). D.D.'s contribution was supported by the Belgian program on Interuniversity Attraction Poles of the Belgian Science Policy (IAP n°P6/19).

REFERENCES.

[1]. Lake R.F., Thompson H., 1970 Proc.Roy.Soc.London **A315** 323.

[2]. Reinke D., Baumgärtel H., Cvitaš T., Klasinc L., Güsten H., 1974 Ber.Bunsen Gesell.Phys.Chem. **78** 1145.

[3]. Reinke D., Krässig R., Baumgärtel H., 1973 Z.Naturf.**28a** 1021.

[4]. Bieri G., Asbrink L., Von Niessen W., 1981 J.Electr.Spectr.Rel.Phenom. **23** 281.

[5]. Bieri G., Von Niessen W., Asbrink L., Svensson A., 1981 Chem.Phys. **60** 61.

[6]. Sze K.H., Brion C.E., Katrib E., El-Issa B., 1989 Chem.Phys. **137** 369.

[7]. Locht R., Leyh B., Hottmann K., Baumgärtel H., 1997 Chem.Phys. **220** 207.

[8]. Hoxha A., Locht R., Leyh B., Dehareng D., Hottmann K., Jochims H.W., Baumgärtel H., 2000 Chem.Phys. **260** 237.

[9]. Locht R., Leyh B., Dehareng D., Jochims H.W., Baumgärtel H., 2009 Chem.Phys. **362** 97.

[10]. Meza S., Wahlgren U., 1971 Theor.Chim.Acta **21** 323.

[11]. Heaton M.M., El-Talbi M.R., 1986 J.Chem.Phys. **85** 7198.

[12]. Potts A.W., Benson J.M., Novak I., Svensson W.A., 1987 Chem.Phys. **115** 253.

[13]. Pradie N.A., Linnert H.V., 2007 J.Phys.Chem.A **111** 4836.

[14]. Takeshita K., 1999 Theor.Chem.Acc. **101** 343.

[15]. Locht R., Leyh B., Hottmann K., Baumgärtel H., 1997 Chem.Phys. **220** 217.

[16]. Reichardt G., Noll T., Packe I., Rotter P., Schmidt J.-S., Gudat W., 2001 Nucl.Instr. and Meth. A **467-468** 458.

[17]. Locht R., Caprace G., Momigny J., 1984 Chem.Phys.Letters **111** 560.

[18]. Locht R., Leyh B., Denzer W., Hagenow G., Baumgärtel H., 1991 Chem.Phys. **155** 407.

[19]. Dunning T.H. Jr, 1989 J.Chem.Phys. **90** 1007.

[20]. Woon D.E., Dunning T.H. Jr., 1993 J.Chem.Phys. **98** 1358.

[23]. Becke A.D., 1993 J.Chem.Phys. **98** 5648.

[22]. Lee C., Wang W., Parr R.G., 1988 Phys.Rev. B **37** 785.

[23]. Foresman J.B., Head-Gordon M., Pople J.A., Frisch M.J., 1992 J.Phys.Chem. **96** 135.

[24]. Hegarty D., Robb M.A., 1979 Mol.Phys. **38** 1795.

[25]. Eade R.H.E., Robb M.A., 1981 Chem.Phys.Letters **83** 362.

[26]. Bernardi F., Bottini A., McDougall J.J.W., Robb M.A., Schlegel H.B., 1984 Faraday Symp.Chem.Soc. **19** 137.

[27]. Frisch M.J., Trucks G.W., Schlegel H.B., Scuseria G.E., Robb M.A.,

Cheeseman J.R., Montgomery J.A. Jr., Vreven T., Kudin K.N., Burant J.C., Millam J.M., Iyengar S.S., Tomasi J., Barone V., Mennucci B., Cossi M., Scalmani G., Rega N., Peterson G.A., Nakatsuji H., Hada M., Ehara M., Toyota K., Fukuda R., Hasegawa J., Ishida M., Nakajima T., Honda Y., Kitao O., Nakai H., Klene M., Li X., Knox J.E., Hratchian H.P., Cross J.B., Adamo C., Jaramillo J., Gomperts R., Stratmann R.E., Yazyev O., Austin A.J., Cammi R., Pomelli C., Ochterski J.W., Ayala P.Y., Morokuma K., Voth G.A., Salvador P., Dannenberg J.J., Zakrzewski V.G., Dapprich S., Daniels A.D., Strain M.C., Farkas O., Malick D.K., Rabuck A.D.,. Raghavachari K., Foresman J.B., Ortiz J.V., Cui Q.,. Baboul A.G., Clifford S., Ciolowski J.,. Stefanov B.B., Liu G., Liashenko A., Piskorz P., Komaromi I., Martin R.L., Fox D.J., Keith T., Al-Laham M.A., Peng C.Y., Nanayakkara A., Challacombe M., Gill P.M.W., Johnson B., Chen W., Wong M.W., Gonzalez C., Pople J.A., GAUSSIAN 03, 2003 Revision B.04, Gaussian Inc., Pittsburgh, PA.

[28]. Dannacher J., Schmelzer A., Stadelmann J.-P., Vogt J., 1979 Intern.J.Mass Spectrom. Ion Phys. **31** 175.

[29]. Kaufel R., Ph.D. Thesis, Freie Universität Berlin, 1985.

[30]. Locht R., Leyh B., Dehareng D., Jochims H.W., Baumgärtel H., to be published.

FIGURE CAPTIONS.

FIG.1: Comparison of the HeI-PES and the TPES recorded with the same electron energy analyzer, under the same conditions showing the resolution reducing effect of the photon monochromator settings used in the present experiments.

FIG.2: (a) Threshold photoelectron spectrum (TPES) of C_2H_3F between 10 eV and 32 eV photon energy. (b) HeI photoelectron spectrum (PES) of C_2H_3F at medium resolution. Vertical bars locate the vertical ionization energies.

FIG.3: (a) Threshold photoelectron spectrum (TPES) of C_2H_3F and Constant Ion State (CIS) spectra at 10.55 eV, 13.79 eV, 14.54 eV, 16.71 eV, 17.91 eV and 20.21 eV successively. (b) The photoabsorption spectrum (PAS) of C_2H_3F as measured in the same photon energy range [9]. Shaded areas indicate energy ranges of excited valence and Rydberg states.

FIG.4: Graphical representation and description of the twelve vibrational normal modes of $C_2H_3F^+$ in the C_S symmetry for which the associated wavenumbers have been calculated.

FIG.5: First photoelectronic band of C_2H_3F as observed between 10.25 eV and 11.45 eV and recorded at E_0=0.39 eV of the electron energy analyzer (exp), the result of its deconvolution (dcv) and its vibrational analysis (vertical bars).

FIG.6: (a) Deconvoluted HeI photoelectron spectrum of C_2H_3F between 13 eV and 21

eV and (b) corresponding Δ-plot enhancing the fine structures in the successive bands.

FIG.7: Δ-plot of the HeI-PES of C_2H_3F on an expanded ionization energy scale between (a) 12.9 eV and 15.5 eV and (b) 15.5 eV and 18.5 eV. Vertical bars indicate the vibrational structures and shaded areas with vertical bars locate the fragment appearance energies measured by photoionization mass spectrometry [29].

TABLE 1. Comparison between the vertical ionization energies (eV) of C_2H_3F as obtained by HeI (54.8nm or 21.22 eV), HeII (30.4 nm or 40.8 eV) and threshold photoelectron spectroscopy. For the assignments to molecular orbitals, see references [4,5]. MET = multiple electron transition.

Ioniz. Orb.	HeI/HeII					TPES
[4,5]	[1]	[2]	[4,5]	[6]	This Work	This Work
$\tilde{X}$,2a″$^{-1}$	10.58	10.57	10.63	10.57	10.55	10.57
$\tilde{A}$,7a′$^{-1}$	13.79	13.80	13.8	13.80	13.79	13.76
$\tilde{B}$,6a′$^{-1}$	14.51	14.56	14.5	14.60	14.53	14.56
$\tilde{C}$,1a″$^{-1}$	-	-	-	16.00	16.16	
5a′$^{-1}$	-	16.76	16.7	16.70	16.71	16.64
$\tilde{D}$,4a′$^{-1}$	17.97	17.97	17.9	17.90	17.91	17.84
$\tilde{E}$,3a′$^{-1}$	-	-	-	-	19.67	-
$\tilde{F}$,2a′$^{-1}$	-	20.27	20.2	20.10	20.20	20.18
	-	21.94	-	-	-	22.7
	-	-	24.5	-	-	24.5
	-	-	-	-	-	26.7
						30.1
1a′/MET						

TABLE 2. Optimized geometries of the neutral ground state of C_2H_3F and the first two ionic states of $C_2H_3F^+$ calculated at the B3LYP//cc-pVTZ level. Optimized geometries of the first two excited states $\tilde{A}\,^2A'$ and $\tilde{B}\,^2A'$ of $C_2H_3F^+$ at the CIS//cc-pVTZ level are also included. The internuclear distances R in A and angles ∠ in degrees. For the atomic numbering refer to the figure inserted. Comparison is made with the results reported in ref. [14] for the neutral and ionic ground states.

State	R(C1-C2)	R(C1-F3)	R(C1-H4)	R(C2-H5)	R(C2-H6)
$\tilde{X}\,^1A'$	1.3168	1.3469	1.0809	1.0796	1.0785
[14]	1.312	1.325	1.081	1.082	1.081
$\tilde{X}\,^2A''$	1.4058	1.2699	1.0875	1.0845	1.0829
[14]	1.402	1.249	1.087	1.085	1.083
$\tilde{A}\,^2A'$					
B3LYP	1.3007	1.2644	1.1900	1.1319	1.0828
CIS	1.3141	1.2384	1.1471	1.1317	1.0690
$\tilde{B}\,^2A'$					
CIS	1.3074	1.2671	1.0827	1.1522	1.1340

State	∠(F3-C1-C2)	∠(H4-C1-C2)	∠(H5-C2-C1)	∠(H6-C2-C1)
$\tilde{X}\,^1A'$	122.21	126.02	121.72	119.29
[14]	122.51	125.29	121.31	119.51
$\tilde{X}\,^2A''$	119.11	125.43	120.14	119.40
[14]	119.65	124.53	119.77	119.43
$\tilde{A}\,^2A'$				
B3LYP	143.18	104.39	111.08	131.04
CIS	139.42	99.67	101.07	135.32
$\tilde{B}\,^2A'$				
CIS	124.37	118.92	141.01	143.76

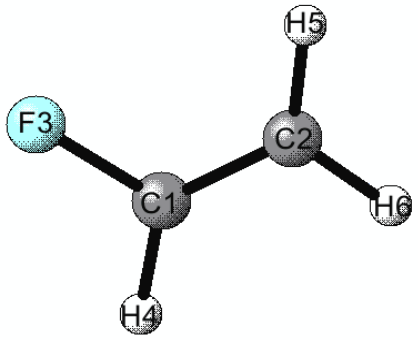

TABLE 3. Optimized geometries at the CAS(12,8) (neutral) or CAS(11,8) (cation) level with (stav) or without (nostav) the state average option for the neutral ground state and the first four ionic states of $C_2H_3F^+$: internuclear distances R in Å and angles ∠ in degrees. For the atomic numbering refer to the figure inserted in Table 2.

State	R(C1-C2)	R(C1-F3)	R(C1-H4)	R(C2-H5)	R(C2-H6)
$\tilde{X}\,^1A'$	1.3401	1.3245	1.0705	1.0719	1.0709
$\tilde{X}\,^2A''$	1.3992	1.2658	1.0764	1.0742	1.0727
$\tilde{A}\,^2A'$	1.3292	1.2417	1.1698	1.1394	1.0678
Stav	1.3229	1.2363	1.2368	1.1090	1.0718
nostav					
$\tilde{B}\,^2A'$	1.3198	1.2747	1.0758	1.1673	1.1542
stav	1.3301	1.2756	1.0804	1.1678	1.1437
nostav					
$\tilde{C}\,^2A''$	1.3343	1.8028	1.0711	1.0744	1.0804
stav	1.3308	1.8318	1.0707	1.0745	1.0813
nostav					

State	∠(F3-C1-C2)	∠(H4-C1-C2)	∠(H5-C2-C1)	∠(H6-C2-C1)
$\tilde{X}\,^1A'$	121.73	125.68	121.41	119.25
$\tilde{X}\,^2A''$	119.73	125.04	120.08	119.16
$\tilde{A}\,^2A'$	139.05	100.49	104.38	133.63
stav	144.83	100.95	109.62	129.67
nostav				
$\tilde{B}\,^2A'$	122.53	120.36	143.87	142.17
stav	123.26	119.21	142.05	141.96
nostav				
$\tilde{C}\,^2A''$	113.83	145.64	123.61	116.17
stav	113.70	146.19	123.90	116.02
nostav				

TABLE 4. Ab initio (B3LYP) calculated wavenumbers (cm^{-1}) associated with the twelve vibrational normal modes (VibrNM) (represented in Fig. 4 for the $C_2H_3F^+$ ($\tilde{X}\ ^2A''$) state) related to the neutral ground state of C_2H_3F and the ionic ground state of $C_2H_3F^+$ respectively. For the atomic numbering in C_2H_3F refer to the figure in Table 2. Comparison is made with previous calculations [14].

This Work		Ref. [14]	
C_2H_3F - $\tilde{X}\ ^1A'$			
VibrNM. a′ Symm.	Wavenbr. (cm^{-1})	Wavenbr. (cm^{-1})	Vibration Norm.Modes Description
ν_1	3 256	3 434	CH Stretch
ν_2	3 197	3 395	CH Stretch
ν_3	3 163	3 333	CH Stretch
ν_4	1 708	1 879	C=C Stretch F-CC & H-CC Bend
ν_5	1 417	1 518	H-CC Bend
ν_6	1 336	1 428	H-CC Bend
ν_7	1 166	1 273	C-F Stretch CH_2 in-plane Rock
ν_8	938	1 023	CH_2 in-plane Rock C-F Stretch
ν_9	489	519	CH_2 in-plane Rock F-CC Bend
a″ Symm.			
ν_{10}	967	-	H out-of-plane Defor.
ν_{11}	899	-	″
ν_{12}	732	-	″

TABLE 4: (continued)

This Work		Ref. [14]	
$C_2H_3F^+$ - $\tilde{X}\ ^2A''$			
Vibr.NM a′ Symm.	Wavenbr. (cm^{-1})	Wavenbr. (cm^{-1})	Vibration Norm.Modes Description
ν_1	3 252	3 450	CH_2 Stretch
ν_2	3 166	3 380	CH4 & CH5 Stretch
ν_3	3 131	3 314	CH_2 & CH4 Stretch
ν_4	1 567	1 737	H-CC Bend C=C & C-F Stretch
ν_5	1 453	1 554	H-CC's Bend
ν_6	1 327	1 413	H4-C-F Bend C-F Stretch
ν_7	1 246	1 337	C=C Stretch F-CC & H-CC Bend
ν_8	984	1 059	CH_2 in-plane Rock C-F Stretch
ν_9	489	521	CH_2 in-plane Rock F-CC Bend
A″ Symm.			
ν_{10}	1 025	-	H out-of-plane Deform.
ν_{11}	873	-	″
ν_{12}	390	-	″

TABLE 5: Ab initio [B3LYP and/or CAS(11,8)] calculated wavenumbers (cm^{-1}) associated with the twelve vibrational motions (VibrNM) (represented in Fig. 4 for the $C_2H_3F^+(\tilde{X}\,^2A'')$ state) related to the $\tilde{A}\,^2A'$, $\tilde{B}\,^2A'$ and $\tilde{C}\,^2A''$ states successively. For the atomic numbering in C_2H_3F refer to the figure in Table 2.

B3LYP		CAS(11,8)	
$C_2H_3F^+ - \tilde{A}\,^2A'$			
VibrNM a′ Symm.	Wavenbr. cm^{-1}	Wavenbr. cm^{-1}	Vibration Norm.Modes Description
ν_1	3 177	3356	C-H_6 Stretch
ν_2	2 643	2909	C_2-H_5 Stretch
ν_3	2 125	1845	C1-H4 Stretch (& C=C & C-F stretch & H4-C1-F bending)
ν_4	1 745	1607	C=C & C-F Stretch or H4-C1 stretch & H4-CC bending
ν_5	1 176	1299	H-CC or CH_2 Bending
ν_6	1 074	1156	CH_2 Bend & C-F Stretch or Stretch C=C, C-F & C1-H4 & Bend H5-C2-F
ν_7	873	920	H4-CC Bend CH_2 in-plane Rock
ν_8	854	701	H4-CC Bend CH_2 in-plane Rock
ν_9	428	286	CH_2 in-plane Rock F-CC Bend
A″ Symm.			
ν_{10}	1 425	1 817	H Out-of-plane Deferm.
ν_{11}	776	803	″
ν_{12}	534	452	″

TABLE 5: (continued).

B3LYP		CAS(11,8)	
$C_2H_3F^+$ - $\tilde{B}\,^2A'$			
Vibr.NM a′ Symm.	Wavenbr. cm^{-1}	Wavenbr. cm^{-1}	Vibration Norm.Modes Description
ν_1	-	3 258	Stretch C1-H4
ν_2	-	2 842	Stretch C2-H sym.
ν_3	-	2 148	Stretch C2-H antisym.
ν_4	-	1 701	Stretch C=C & Stretch C-F & Stretch H5-C2 & Bending H4-CC
ν_5	-	1 359	Bendings H-CC
ν_6	-	1 316	Bending H5,H6-CCH & Stretch C-F
ν_7	-	1 094	Bending H-CC
ν_8	-	529	CH_2 rock in-plane & Bendings
ν_9	-	326	CH_2 rock in-plane
A″ Symm.			
ν_{10}	-	1 680	H out-of-plane Deform.
ν_{11}	-	876	"
ν_{12}	-	387	"

TABLE 5: (continued)

B3LYP		CAS(11,8) TS in C_S Symm.Group	
$C_2H_3F^+$ - $\tilde{C}\,^2A''$			
VibrNM. a′ Symm.	Wavenbr. cm^{-1}	Wavenbr. cm^{-1}	Vibration Norm.Modes Description
ν_1	-	3 409	Stretch C1-H4
ν_2	-	3 371	Stretch C2-H antisym.
ν_3	-	3 241	Stretch C2-H sym.
ν_4	-	1 793	Stretch C=C & Bendings H-CC
ν_5	-	1 474	Bendings H-CC
ν_6	-	1 276	Bending H-C-H
ν_7	-	892	Bending H4-CC & CH_2 rock in-plane
ν_8	-	500	Stretch C-F & CH_2 rock in-plane
ν_9	-	313	CH_2 rock in-plane & Bending F-CC
a″ Symm.			
ν_{10}	-	1 003	H out-of-plane Deformation
ν_{11}	-	566	"
ν_{12}	-	*i 1 751*	"

TABLE 6. Optimized geometries of the $\tilde{A}\,^2A'$ / $\tilde{B}\,^2A'$ states avoided crossing (AC) and of the $\tilde{B}\,^2A'/\tilde{C}\,^2A''$ and $\tilde{C}\,^2A''/\tilde{D}\,^2A'$ states conical intersections (CI). Internuclear distances R in Å and angles in degrees. For the atomic numbering refer to the figure in Table 2.

Calc.	State	R(C1-C2)	R(C1-F3)	R(C1-H4)	R(C2-H5)	R(C2-H6)
CIS	$\tilde{A}\,^2A'$ $\tilde{B}\,^2A'$	1.3141 1.3074	1.2384 1.2671	1.1471 1.0827	1.1317 1.1522	1.0690 1.1340
CAS (7,7)	AC $\tilde{A}/\tilde{B}$	1.3681	1.2499	1.1056	1.1131	1.1792
CAS (11,8)	AC $\tilde{A}/\tilde{B}$	1.3841	1.2531	1.1021	1.0921	1.1453
	CI $\tilde{B}/\tilde{C}$	1.3304	1.8474	1.0738	1.0774	1.0798
	CI $\tilde{C}/\tilde{D}$	1.2906	2.0373	1.0765	1.0772	1.0824

Calc.	State	∠(F3-C1-C2)	∠(H4-C1-C2)	∠(H5-C2-C1)	∠(H6-C2-C1)
CIS	$\tilde{A}\,^2A'$ $\tilde{B}\,^2A'$	139.42 124.37	99.67 118.92	101.07 141.01	135.32 143.76
CAS (7,7)	AC $\tilde{A}/\tilde{B}$	119.52	119.59	127.22	110.51
CAS (11,8)	AC $\tilde{A}/\tilde{B}$	119.66	120.91	128.84	113.08
	CI $\tilde{B}/\tilde{C}$	111.39	149.00	122.54	117.35
	CI $\tilde{C}/\tilde{D}$	116.24	129.76	121.75	116.28

TABLE 7. Energy position (eV), tentative assignments and predicted level (eV) for the structures observed in the first photoelectronic band corresponding to the $C_2H_3F^+(\tilde{X}\ ^2A'')$ state: (0,0) means vibrationless level. Comparison is made with the TPES measured in this work.

HeI-PES	TPES	Assignment
10.363	10.367	(0,0)
10.424	10.419	ν_9 (10.424)
10.466	10.475	ν_8
10.485	-	$2\nu_9$ (10.485) or ν_8 (10.485)
10.523	10.523	ν_7 (10.517)
10.558	10.551	ν_4 (10.557)[or $3\nu_9$ (10.546)]
10.570	-	$2\nu_8$
10.586	-	$\nu_7+\nu_9$ *(10.578)*
10.610	10.607	$4\nu_9$ (10.603) or $2\nu_8$ (10.607)
10.619	-	$\nu_4+\nu_9$ (10.618)
10.641	-	$\nu_7+\nu_8$ *(10.639)*
10.655	10.655	$\nu_4+\nu_8$
10.674	-	$3\nu_8$
10.679	10.679	$\nu_4+2\nu_9$ or $\nu_4+\nu_8$ (10.679)
10.714	10.711	$\nu_4+\nu_7$
10.740	10.739	$\nu_4+3\nu_9$
10.749	-	$2\nu_4$ (10.751)
10.767	10.759	$\nu_4+2\nu_8$
10.779	-	$\nu_4+\nu_7+\nu_9$ *(10.762)*
10.801	10.803	$\nu_4+4\nu_9$ or $\nu_4+2\nu_8$ (10.801)
10.810	-	$2\nu_4+\nu_9$
10.830	-	$\nu_4+\nu_7+\nu_8$ *(10.833)*
10.842	-	$2\nu_4+\nu_8$
10.866	10.860	$2\nu_4+2\nu_9$
10.897	-	na
10.907	10.904	$2\nu_4+\nu_7$
10.927	10.928	$2\nu_4+3\nu_9$
10.944	10.948	$3\nu_4$ (10.945)
10.954	-	$2\nu_4+2\nu_8$
10.970	-	na

TABLE 7: (continued).

10.992	-	$2\nu_4+2\nu_8$ (10.995)
11.003	-	$3\nu_4+\nu_9$
11.019	~11.01	$2\nu_4+\nu_7+\nu_8$ *(11.027)*
11.045	-	$3\nu_4+\nu_8$
11.059	~11.05	$3\nu_4+2\nu_9$
11.075	-	$3\nu_4+2\nu_8$ (11.067)
11.096	~11.09	$3\nu_4+\nu_7$
11.114	-	$3\nu_4+\nu_8+\nu_9$ *(11.110)*
11.137	~11.14	$4\nu_4$ (11.139)
11.151	-	$3\nu_4+2\nu_8$
11.167	-	$3\nu_4+\nu_7+\nu_9$ *(11.160)*
11.183	-	$3\nu_4+2\nu_8$ (11.189)
11.197	-	$4\nu_4+\nu_9$
11.216	-	$3\nu_4+\nu_7+\nu_8$ *(11.221)*
11.232	-	$4\nu_4+\nu_8$
11.254	-	$3\nu_4+3\nu_8$
11.264	~11.26	$4\nu_4+2\nu_9$
11.279	-	na
11.295	-	$4\nu_4+\nu_7$
11.321	-	$4\nu_4+3\nu_9$
11.333	-	$5\nu_4$ (11.333)
11.352	-	na
11.372	-	na
11.392	-	$5\nu_4+\nu_9$
11.409	-	$4\nu_4+\nu_7+\nu_8$ *(11.415)*
11.423	-	na
11.443	-	$5\nu_4+\nu_8$
11.459	-	$5\nu_4+2\nu_9$ or $5\nu_4+\nu_8$ (11.455)
11.470	-	na
11.492	-	$5\nu_4+\nu_7$
11.508	-	$5\nu_4+3\nu_9$ (11.516)
11.526	-	$5\nu_4+3\nu_9$
11.545	-	$5\nu_4+2\nu_8$
11.565	-	$5\nu_4+2\nu_8$ (11.577)

TABLE 8. Comparison of the vibrational wavenumbers (cm^{-1}) characterizing the $C_2H_3F^+$ ($\tilde{X}\ ^2A''$) band in the HeI-PES as reported in previous works, in the present work and those predicted by ab initio quantum mechanical calculations in this work and in ref.[14].

Experiment					Theory	
Vibr. N.M.	[1]	[2]	[6]	This Work	[14]	This Work
ν_4	1530	1570	1530	1565±16	1737	1567
ν_7	1330	1330	1270	1278±128	1337	1246
ν_8	-	-	850	39±40[a] or 968±30[a]		
				500±32	1059	984
ν_9	510	500	500		521	489

[a] For the discussion, see text.

TABLE 9. Energy position (eV) of the fine structures observed in the second to seventh photoelectron bands of C_2H_3F and their assignments.

State	Energy (eV)	Assignment(s)
$\tilde{A}\,^2A'$	12.953	$IE_{ad}(0,0)$
	13.014	ν_9
	13.083	ν_A[a]
	13.143	$\nu_9+\nu_A$
	13.203	$2\nu_A$
	13.253	$\nu_9+2\nu_A$
	13.313	$3\nu_A$
	13.363	$\nu_9+3\nu_A$
	13.413	$4\nu_A$
	(13.443)	na
	13.513	$5\nu_A$
	13.563	$\nu_9+5\nu_A$
	13.653	na
	13.703	na
	13.783	na
	13.873	na
	13.952	$n\nu_A$
	14.013	$(n+1)\nu_A$
	14.102	$(n+2)\nu_A$
	(14.192)	na
	14.232	$(n+3)\nu_A$
$\tilde{B}\,^2A'$	14.342	E_{min}
	14.442	$E_{min}+\nu_7$
	14.532	$E_{min}+2\nu_7$
	14.672	- $+3\nu_7$
	14.872	- $+5\nu_7$
	14.992	- $+6\nu_7$
	15.121	- $+7\nu_7$
	15.221	- $+8\nu_7$
	15.271	- $+9\nu_7$
	15.321	- $+10\nu_7$

TABLE 9: (continued).

State	Energy (eV)	Assignment(s)
$\tilde{C}\,^2A''$	15.511	E_{min}
	15.581	$E_{min}+\nu_8$
	15.681	- $+\nu_B$
	15.751	$E_{min}+\nu_4$
	15.821	$E_{min}+\nu_4+\nu_8$
	15.871	- $+\nu_4+\nu_B$
	15.971	$E_{min}+2\nu_4$
	16.060	$E_{min}+2\nu_4+\nu_8$
	16.120	- $+2\nu_4+\nu_B$
$\tilde{D}\,^2A'$	16.300	E_{min}
	16.400	$E_{min}+\nu_C$
	16.450	$E_{min}+\nu_B$
	16.520	$E_{min}+\nu_A$
	16.590	- $+\nu_A+\nu_C$
	(16.660)	- $+\nu_A+\nu_B$
	16.730	$E_{min}+2\nu_A$
	16.810	- $+2\nu_A+\nu_C$
	16.930	$E_{min}+3\nu_A$
	17.000	- $+3\nu_A+\nu_C$
	17.050	- $+3\nu_A+\nu_B$
	17.109	$E_{min}+4\nu_A$
	17.189	- $+4\nu_A+\nu_C$
	17.269	- $+4\nu_A+\nu_B$
	17.299	$E_{min}+5\nu_A$
$\tilde{E}\,^2A'$	17.414	na
	17.459	E_{min}
	17.549	$E_{min}+\nu_A$
	17.589	- $+\nu_9$
	17.649	$E_{min}+2\nu_A$

TABLE 9: (continued).

State	Energy (eV)	Assignments
$\tilde{E}\,^2A'$	17.709	$E_{min}+2\nu_A+\nu_9$
	17.758	$E_{min}+3\nu_A$
	17.809	- $+3\nu_A+\nu_9$
	17.849	$E_{min}+4\nu_A$
	17.889	- $+4\nu_A+\nu_9$
	17.949	$E_{min}+5\nu_A$
	17.998	- $+5\nu_A+\nu_9$
	18.068	E_{min}'
	18.133	$E_{min}'+\nu_9$
	18.188	$E_{min}'+\nu_C$
	18.238	- $+\nu_C+\nu_9$
	18.308	$E_{min}'+2\nu_C$
	18.363	- $+2\nu_C+\nu_9$
	18.438	$E_{min}'+3\nu_C$
$\tilde{G}\,^2A'$	19.917	na
	20.026	E_{min}
	20.156	$E_{min}+\nu_A$
	20.266	- $+2\nu_A$
	20.386	- $+3\nu_A$
	20.506	- $+4\nu_A$
	20.636	- $+5\nu_A$

[a] na= not assigned.
For the designation and assignment of ν_A, ν_B, ν_C and see text.

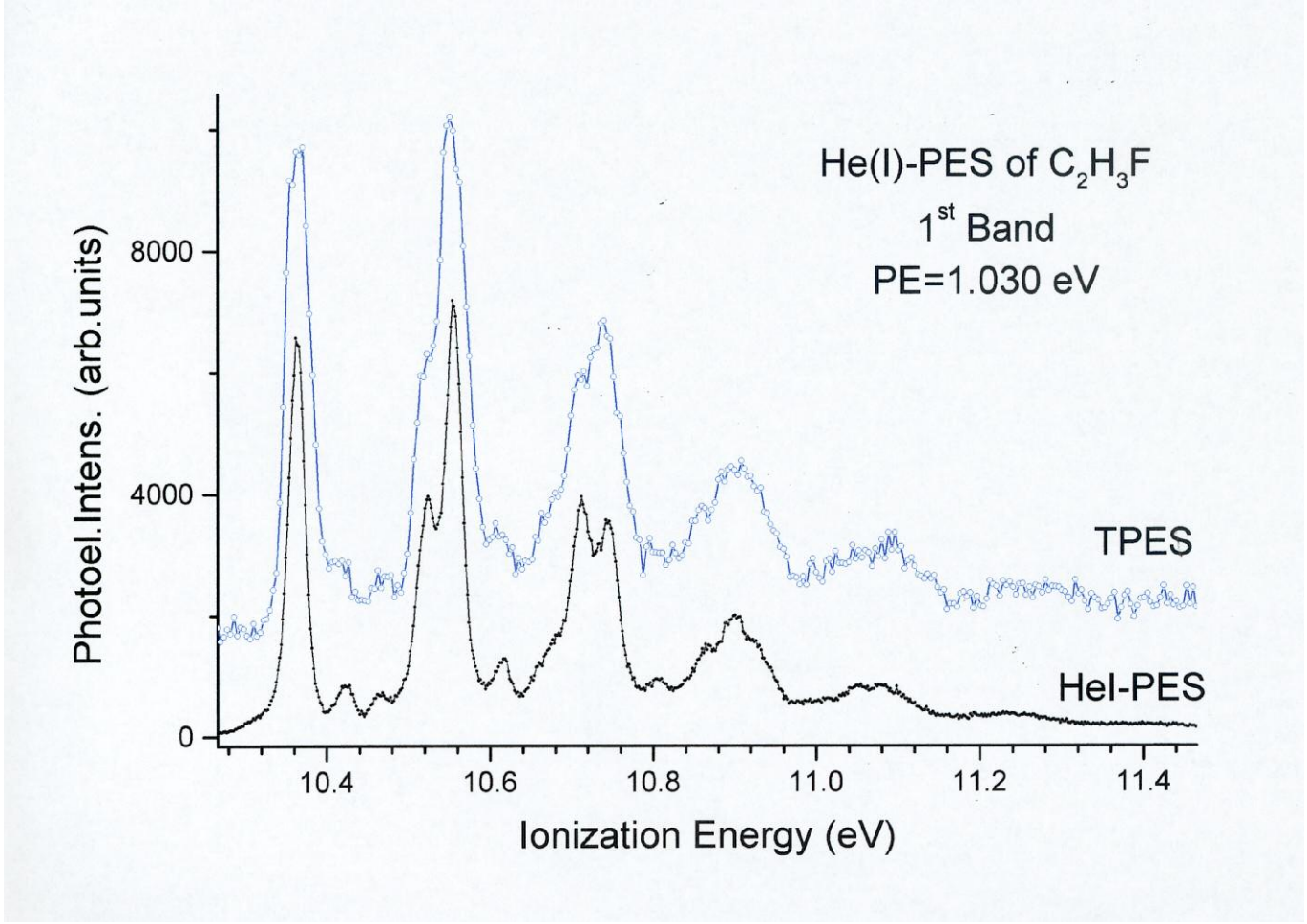

Figure 1 (C2H3F-002Fig1.tif)

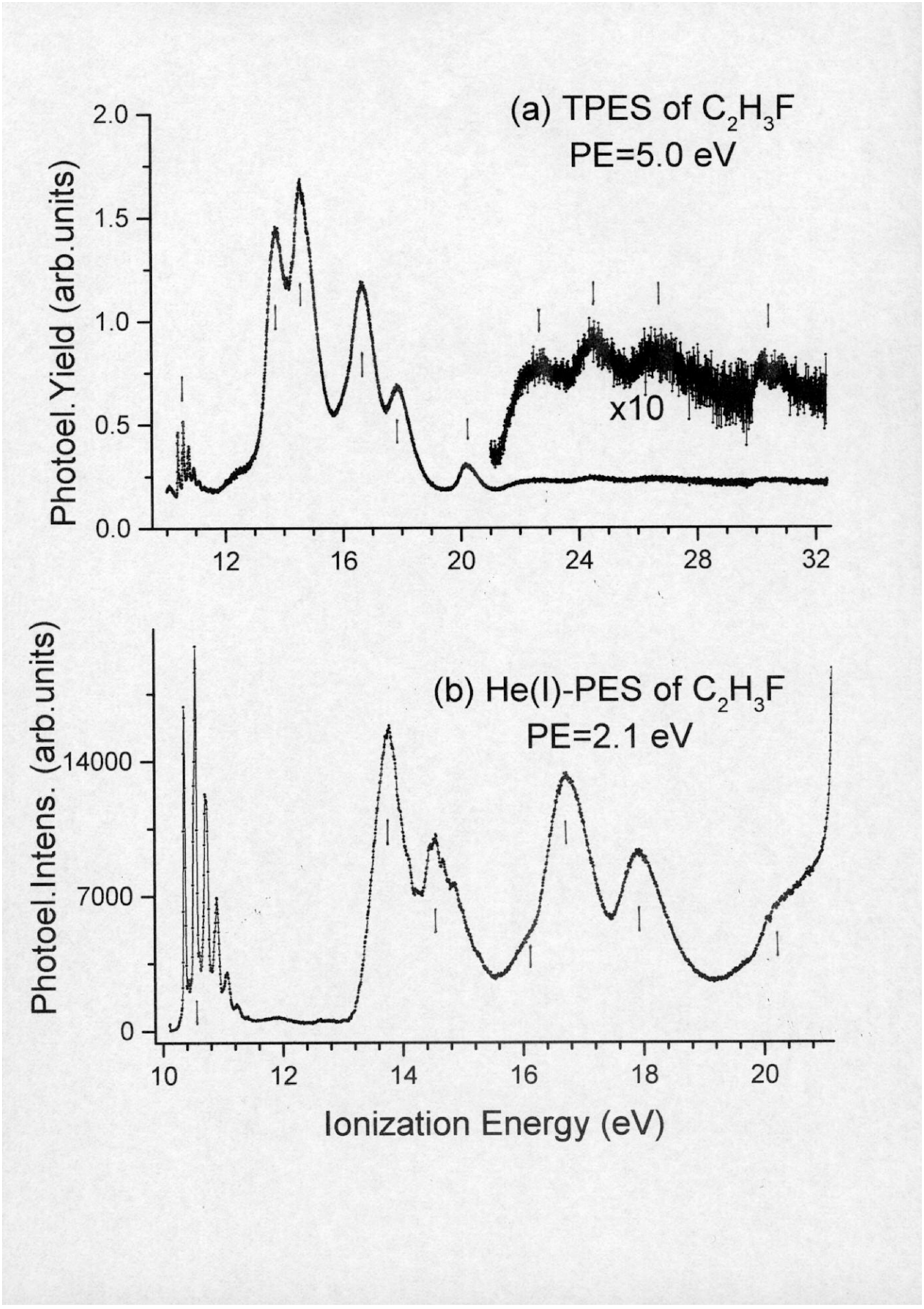

Figure 2 (C2H3F-002Fig2.tif)

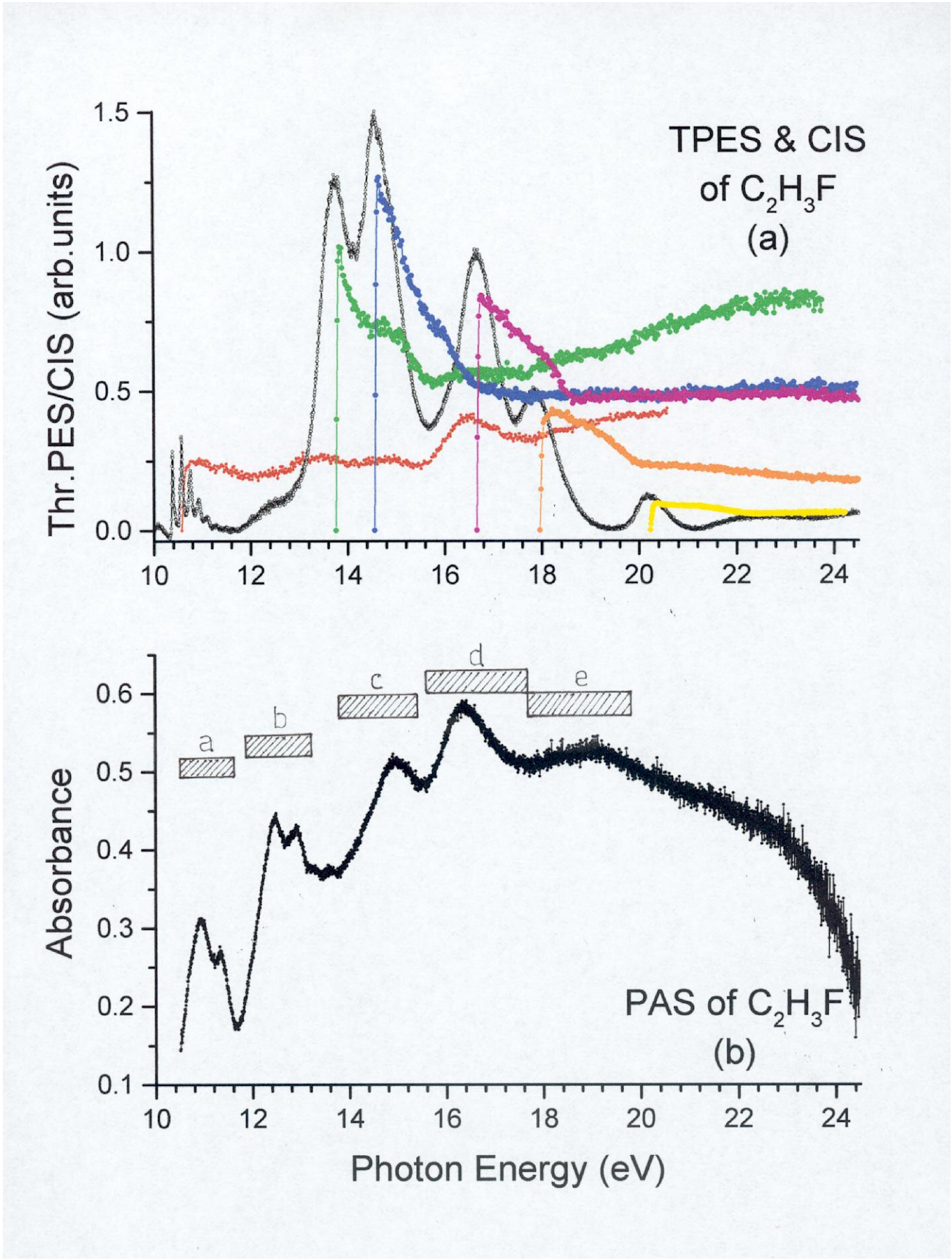

Figure 3 (C2H3F-002Fig3.tif)

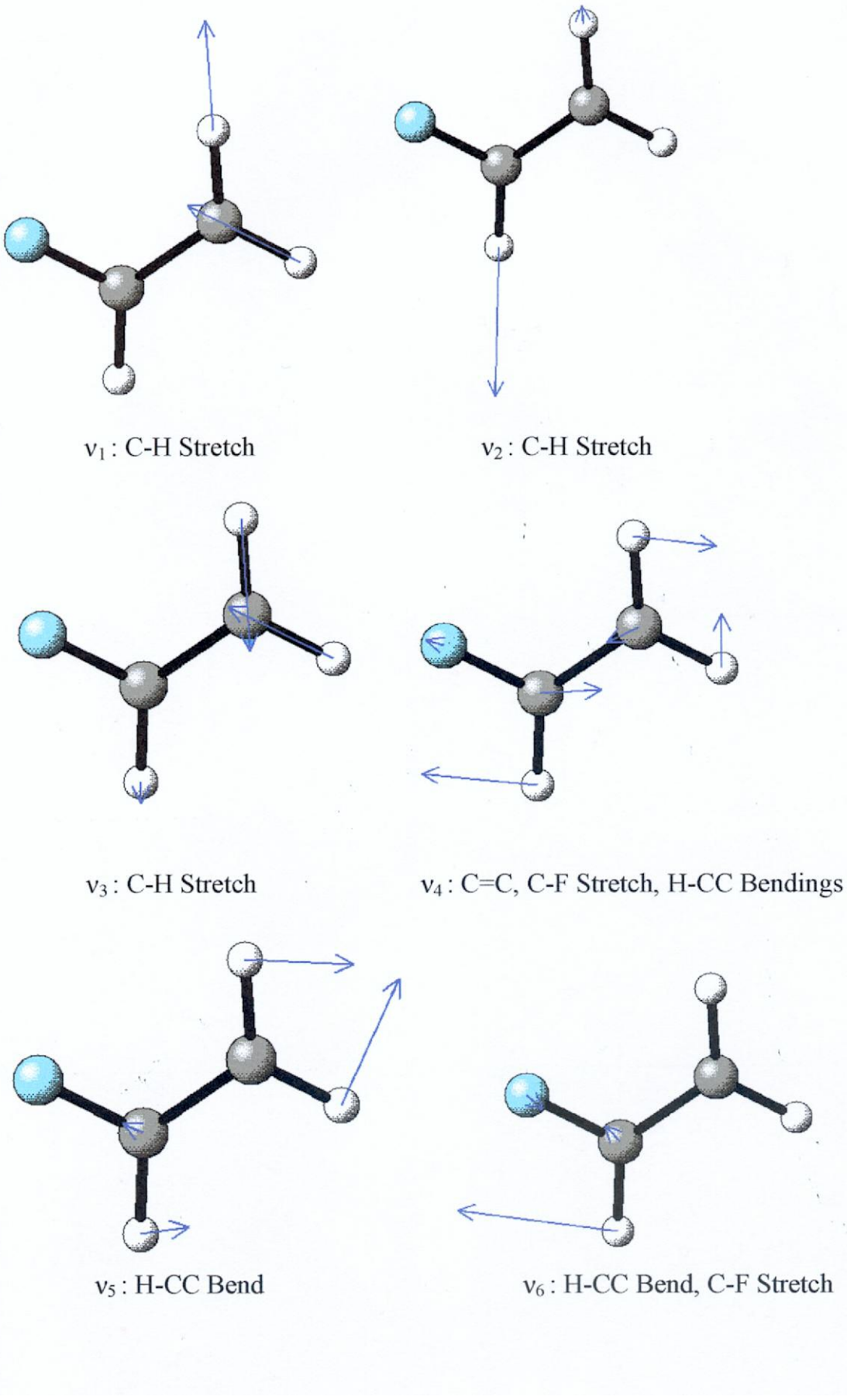

Figure 4a (C2H3F-002Fig4(1).tif)

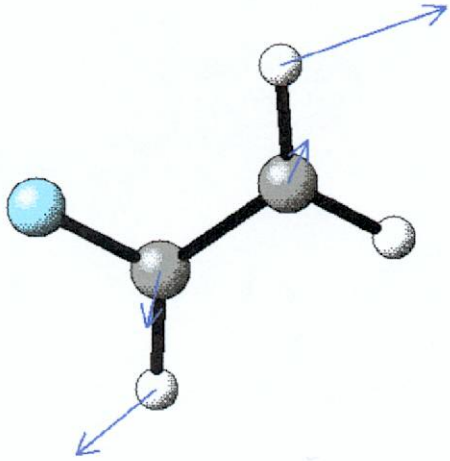

ν_7 : C=C Stretch, H-CC Bend

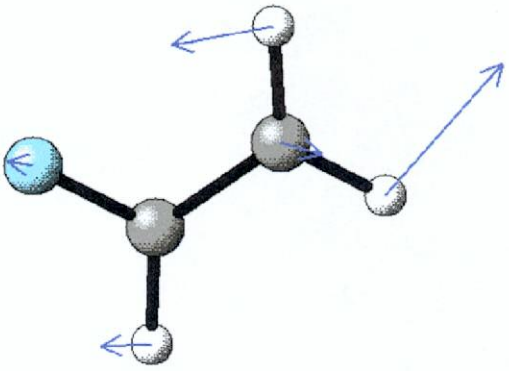

ν_8: C-F Stretch, CH_2 Rock in-plane

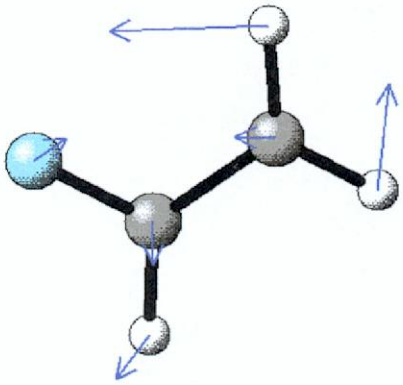

ν_9 : Bend F-CC, CH_2 Rock in-plane

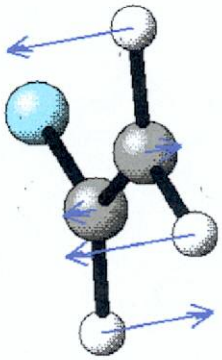

ν_{10} : Out-of-plane Deformation

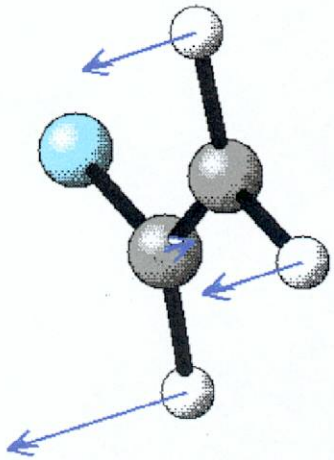

ν_{11} : Out-of-plane Deformation

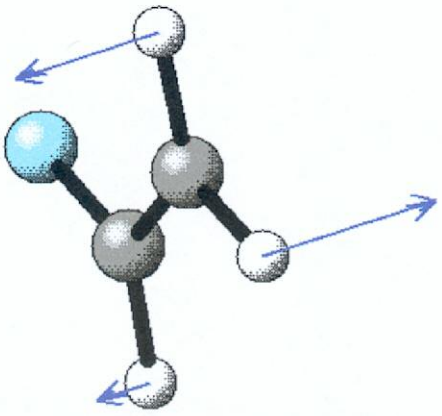

ν_{12}: Out-of-plane Deformation

Figure 4b (C2H3F-002Fig4(2).tif)

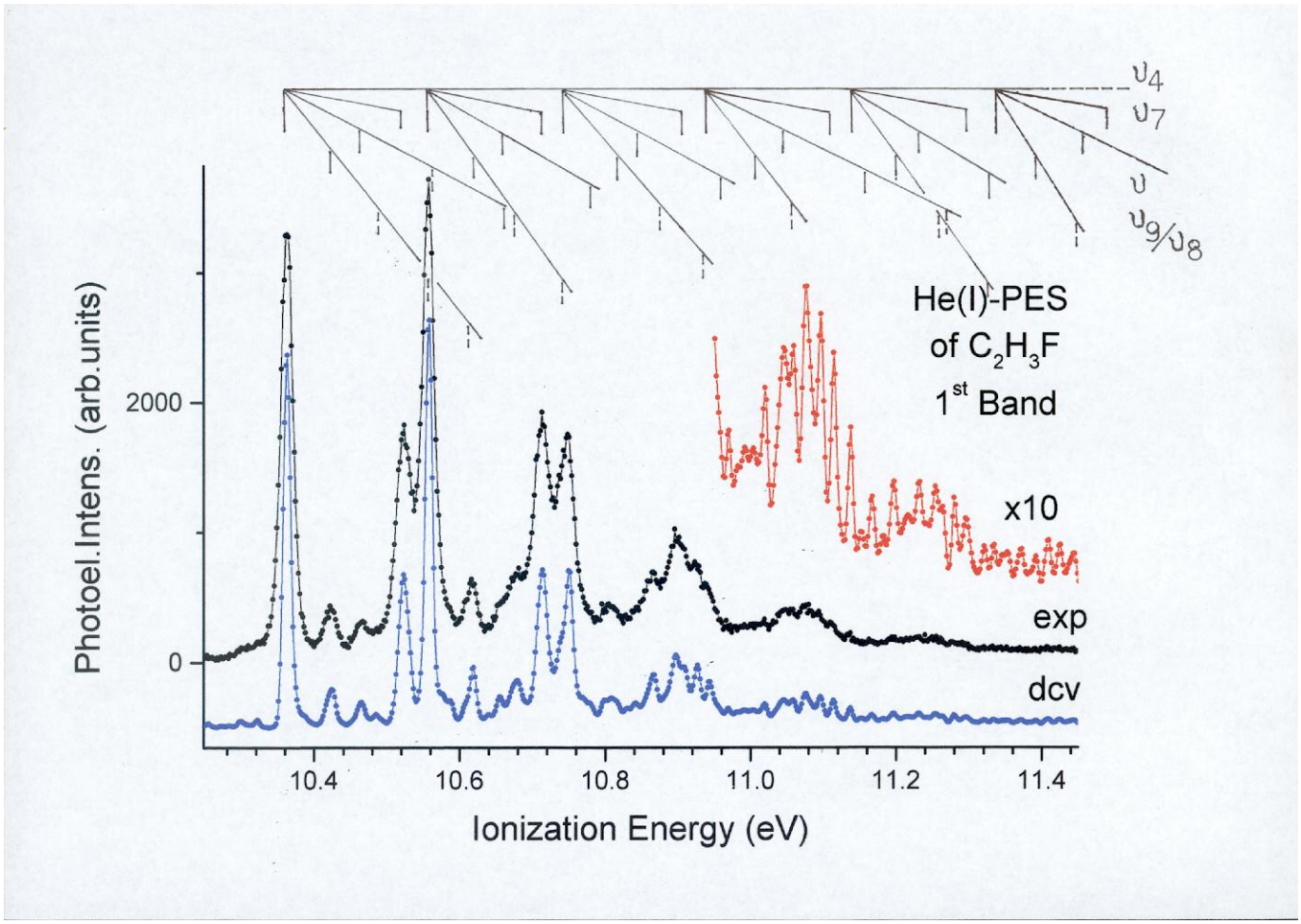

Figure 5 (C2H3F-002Fig5.tif)

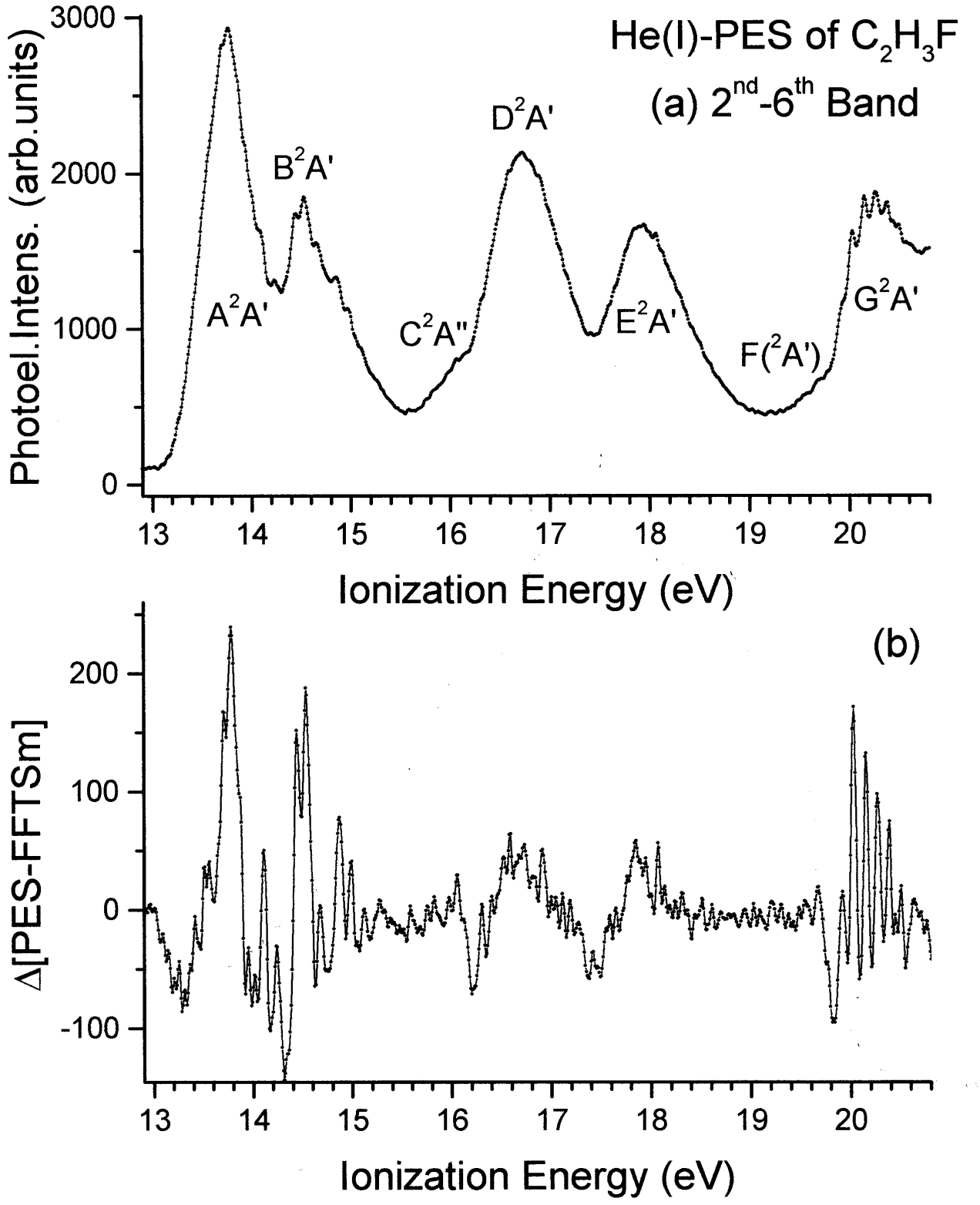

Figure 6 (C2H3F-002Fig6.tif)

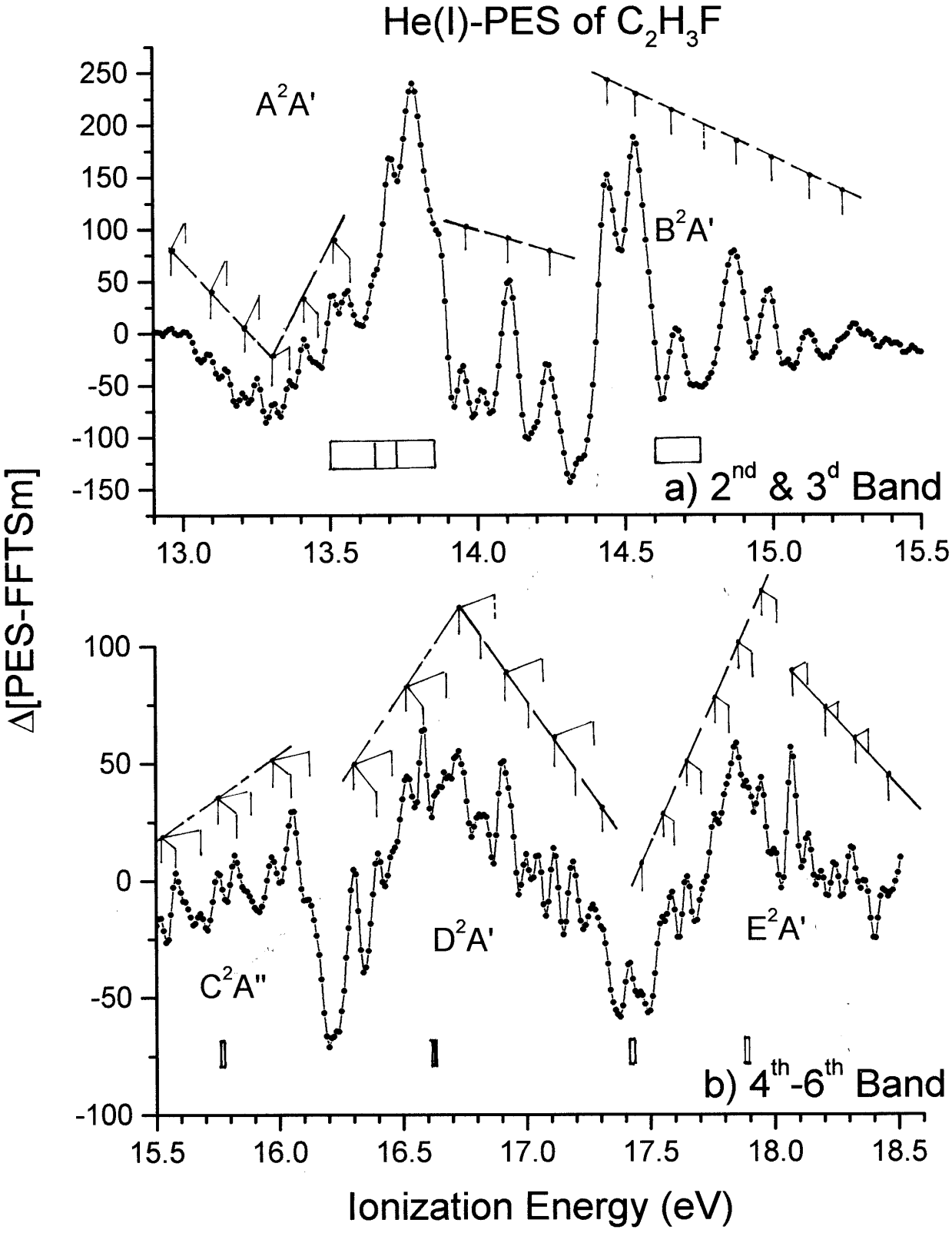

Figure 7 (C2H3F-002Fig7.tif)